

# 9 Strongly Correlated Electrons: Estimates of Model Parameters

Olle Gunnarsson

Max-Planck-Institut für Festkörperforschung

Heisenbergstraße 1, 70569 Stuttgart, Germany

## Contents

<b>1</b>	<b>Introduction</b>	<b>2</b>
<b>2</b>	<b>Projecting out states</b>	<b>4</b>
2.1	One-particle Hamiltonian . . . . .	4
2.2	Many-body Hamiltonian . . . . .	5
<b>3</b>	<b>Effective Coulomb interaction</b>	<b>7</b>
3.1	Perfect screening . . . . .	8
3.2	Constrained density functional formalism . . . . .	8
3.3	Constrained RPA . . . . .	9
3.4	Screening and breathing . . . . .	10
3.5	Results . . . . .	11
<b>4</b>	<b>Neglected renormalizations</b>	<b>11</b>
4.1	Configuration dependence of hopping integrals . . . . .	11
4.2	Many-body renormalization of hopping integrals . . . . .	13
<b>5</b>	<b>Fullerenes</b>	<b>16</b>
5.1	Hopping . . . . .	16
5.2	Coulomb interaction . . . . .	18
5.3	Electron-phonon interaction . . . . .	19
<b>6</b>	<b>Conclusions</b>	<b>23</b>

# 1 Introduction

For weakly or moderately correlated systems *ab initio* methods, such as the density functional formalism [1, 2] or the GW method [3, 4], are often quite successful. For strongly correlated systems, however, these methods are often not sufficient. It is then necessary to treat correlation effects in a more accurate way. Such systems are often quite complicated with large unit cells. It is then very hard to treat correlation effects within an *ab initio* approach, and one often turns to model Hamiltonians. The idea is then to focus on states and interactions believed to be particularly important for the physics of interest. This has the additional advantage that it may then be easier to understand the physics, since less important effects do not confuse the interpretation. On the other hand, there is a risk of oversimplifying the model and thereby missing the correct physics. The purpose of this lecture is to discuss this approach.

In principle it is straightforward to construct a model. We can produce a complete basis set and then calculate matrix elements of the real space Hamiltonian (in atomic units)

$$H = \sum_i \left( -\frac{1}{2} \nabla_i^2 + V_{ext}(\mathbf{r}_i) \right) + \sum_{i < j} \frac{1}{|\mathbf{r}_i - \mathbf{r}_j|}. \quad (1)$$

For atoms or small molecules, this Hamiltonian may then be solved using various many-body methods, e.g., configuration interaction (CI), where the many-body wave function is written as a linear combination of determinants. For strongly correlated solids, however, a Hamiltonian obtained in this way is often too complicated to allow reasonably accurate calculations. We are then forced to use substantially simpler models. This usually involves a drastic reduction of the basis set and the neglect of many interactions. Typical examples are the Anderson [5], the Hubbard [6] and the *t*-*J* [7] models.

This approach involves the neglect of interactions which are large. For instance, the Anderson impurity model is often used for a *3d* impurity in a weakly correlated host. We define a direct Coulomb integral

$$F_{ij} = \int d^3r \int d^3r' \frac{|\Phi_i(\mathbf{r})|^2 |\Phi_j(\mathbf{r}')|^2}{|\mathbf{r} - \mathbf{r}'|}, \quad (2)$$

where  $\Phi_i(\mathbf{r})$  is the wave function of a state *i*. Then the Coulomb integral  $F_{3d,3d}$  between *3d* electrons is kept, while, for instance, the integral  $F_{3d,4s}$  between a *3d* and a *4s* electron is neglected. For a free Mn atom  $F_{3d,3d} = 21$  eV and  $F_{3d,4s} = 10$  eV. Such an approximation is clearly highly questionable. An essential task is then to try to include the explicitly neglected interactions or states implicitly as a renormalization of parameters in the model. As we show later, this leads to an effective Coulomb interaction between the *3d* electrons which is much smaller than the calculated value for a free atom. A basic assumption of such simple models is then that all the neglected interactions can, with a reasonable accuracy, be included implicitly as a renormalization of various model parameters. In this approach it is important to keep track of what effects are explicitly included in the model. These should not be included in the calculation of renormalized parameters, since this would involve double-counting.

There are various ways of obtaining parameters. One approach has been indicated above. We use *ab initio* calculations to calculate parameters and then we try to estimate how these are

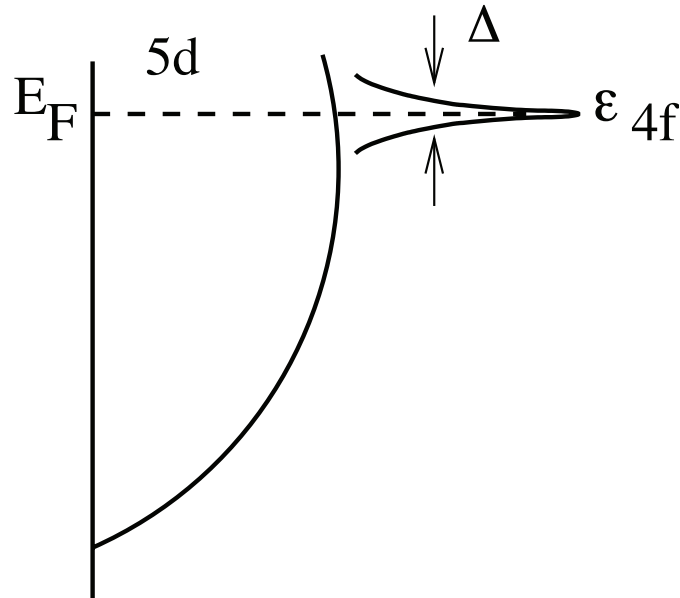


**Fig. 1:** Schematic density of state for a Ce compound according to the promotional model.

renormalized by neglected interactions. Another is to calculate certain properties of the model, compare with experiment and then adjust parameters until the experimental value is obtained. This approach then automatically gives renormalized parameters. It is important to try to obtain as much independent information as possible about the parameters, both from calculations and from different experiments, and to check if the various pieces of information are consistent.

The importance of obtaining theoretical information about parameters can be illustrated by the historical development of the theory of Ce compounds. Traditionally, Ce compounds were described in the so called promotional model [8]. It was assumed that the Ce  $4f$  level was located very close to the Fermi level,  $E_F$ , and that it had a very weak interaction with other states. A mean-field theory was then used to show that this leads to a very narrow resonance, as indicated in Fig. 1. The narrowness of the resonance could explain the large susceptibility and specific heat of Ce compounds, and the closeness of the  $4f$  level to  $E_F$  the change of apparent valence when the pressure or temperature are changed. Thermodynamic considerations, however, showed that the  $4f$  level ought to be about 2 eV below  $E_F$  [9], in strong disagreement with the model. This result was later reconciled with experiment in a many-body approach [10, 11], showing that even if the  $4f$  level is far below  $E_F$  it can form a Kondo-like many-body resonance at  $E_F$  leading to very large values of the susceptibility and the specific heat. This illustrates how an oversimplified (mean-field) method can nevertheless lead to reasonable results if it is combined with a bad choice of parameters. Correcting the parameters then forces us to use a better method and to find out more about the correct physics.

## 2 Projecting out states

### 2.1 One-particle Hamiltonian

One approach to the construction of models is to project out states which are believed not to be essential for the physics. We can illustrate this for a one-particle Hamiltonian

$$H = \sum_i \varepsilon_i n_i + \sum_{i \neq j} t_{ij} \psi_i^\dagger \psi_j \quad (3)$$

We introduce a projection operator

$$P = \sum_{\nu \in P} |\nu\rangle \langle \nu|, \quad (4)$$

where  $|\nu\rangle$  are states we want to keep. We introduce the resolvent operator

$$(z - H)^{-1} = \sum_{\nu} |\nu\rangle \langle \nu| (z - H)^{-1} \sum_{\mu} |\mu\rangle \langle \mu| = \sum_n |n\rangle \frac{1}{z - E_n} \langle n|, \quad (5)$$

which has poles for  $z = E_n$  at the eigenvalues, where  $H|n\rangle = E_n|n\rangle$ . Introducing the complement  $Q = (1 - P)$ , we can write the Hamiltonian as [12, 13]

$$\begin{pmatrix} H_{PP} & H_{PQ} \\ H_{QP} & H_{QQ} \end{pmatrix}, \quad (6)$$

where, e.g.,  $H_{PP} = PHP$ . Then we can derive the exact result (Löwdin downfolding)

$$P(z - H)^{-1}P = [z - H_{PP} - H_{PQ}(z - H_{QQ})^{-1}H_{QP}]^{-1}. \quad (7)$$

The operator  $P(z - H)^{-1}P$  has the same poles as the original operator  $(z - H)^{-1}$ , if the corresponding eigenstates have weight inside the space  $P$ . The new operator has a smaller dimension, but because of the  $z$  dependence it is not simpler. To simplify the expression, we put  $z$  equal to an energy ( $\varepsilon_0$ ) in the range of interest. The operator is then energy independent. As an additional simplification, we may assume that the off-diagonal elements of  $H_{QQ}$  can be neglected. Then the matrix elements of the new operator become

$$t_{ij} \rightarrow t_{ij} - \sum_{\mu \in Q} \frac{t_{i\mu} t_{\mu j}}{\varepsilon_0 - E_\mu}. \quad (8)$$

This latter approximation is accurate if the states being projected out are much higher in energy than the states of interest and if the off-diagonal elements are small compared with the energy difference  $\varepsilon_0 - E_\mu$ . The assumption about  $H_{QQ}$  being diagonal can also be relaxed. This approach reduces the size of the Hamiltonian matrix, i.e., the number of states, at the cost of obtaining more long-range hopping. For a one-particle Hamiltonian, this approach is a controlled and systematic procedure for reducing the size of the Hamiltonian.

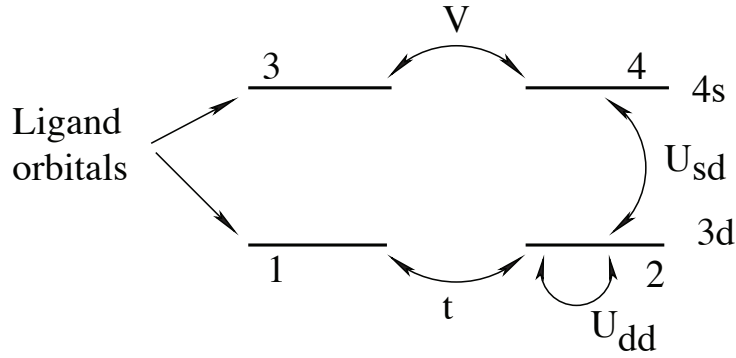


**Fig. 2:** Schematic picture of a very simple model of a transition metal compound, with a  $3d$  atom (levels 2 and 4) coupling to a ligand (with levels 1 and 3).

## 2.2 Many-body Hamiltonian

We now consider a many-body Hamiltonian, with a two-body interaction in the form of a Coulomb interaction. We then define  $P$  as projecting out states that have no electron in certain (high-lying) one-particle states  $|\mu\rangle$ , and  $Q = 1 - P$ . We consider a Coulomb interaction with four (creation and annihilation) operators and project out a state with one electron in  $|\mu\rangle$ . Then  $H_{QP}$  contains an operator  $c_{\mu\sigma}^\dagger$  and  $H_{PQ}$  an operator  $c_{\mu\sigma}$ . Even if we assume  $H_{QQ}$  to be diagonal, we are left with an operator  $H_{PQ}H_{QP}$  acting on a state without electrons in  $|\mu\rangle$ . Then  $c_{\mu\sigma}c_{\mu\sigma}^\dagger \equiv 1$ , and two operators drop out. But we are still left with six other operators, which in the general case are all different. We have then generated a three-body operator. This is too complicated, and all such operators need to be neglected. Unless it can be shown that these terms are small, this means that there is not a controlled systematic procedure for reducing the number of states. We then have to rely on more intuitive approaches.

As an example we consider a very simple model which is relevant for  $3d$  impurities. The model is constructed so that an exact solution can be found. We want to illustrate how this model can be projected down to a simpler model with renormalized parameters. We introduce the Hamiltonian [14]

$$H = \sum_{\sigma} \left( \sum_{i=1}^4 \varepsilon_i n_{i\sigma} + (t\psi_{1\sigma}^\dagger \psi_{2\sigma} + V\psi_{3\sigma}^\dagger \psi_{4\sigma} + \text{H.c.}) \right) + U_{dd} n_{2\uparrow} n_{2\downarrow} + U_{sd} \sum_{\sigma\sigma'} n_{2\sigma} n_{4\sigma'} \quad (9)$$

where level 2 corresponds to a  $3d$  level and level 4 to a  $4s$  level on a transition metal atom. Level 1 and 3 correspond to a ligand coupling to the transition metal atom via the hopping integrals  $t$  and  $V$ . On the transition metal atom there is a large Coulomb interaction  $U_{dd}$  between electrons in the  $3d$  level and a weaker  $U_{sd}$  interaction between the  $3d$  and  $4s$  levels. We assume that orbital 2 is quite localized, so that  $t$  is small, but that levels 3 and 4 are delocalized, so that  $V$  is large. The level structure is shown schematically in Fig. 2.

We first consider the spinless case, and put one electron in each of the spaces 1+2 and 3+4. We derive parameters in an intuitive approach, and then compare with a controlled projection approach, possible in this case. We introduce the eigenstates of the space 3+4 with the electron in space 1+2 on site 1 or 2. With the electron on level 1 the bonding and antibonding eigenstates

in the 3+4 space are

$$\psi_{b1} = a_3\psi_3 + a_4\psi_4 \quad (10)$$

$$\psi_{a1} = a_4\psi_3 - a_3\psi_4,$$

with the energies  $\varepsilon_{b1}$  and  $\varepsilon_{a1}$ . With the electron in 1+2 on level 2 the states are

$$\psi_{b2} = \cos\phi \psi_{b1} + \sin\phi \psi_{a1} \quad (11)$$

$$\psi_{a2} = \sin\phi \psi_{b1} - \cos\phi \psi_{a1}, \quad (12)$$

$$(13)$$

with the energies  $\varepsilon_{b2}$  and  $\varepsilon_{a2}$ . Here  $\phi$  is of the order  $U_{sd}/V$  which is small in the limit we consider below. We assume that the electron in the space 3+4 can adjust completely to the movement of the electron in space 1+2 due to  $|V| \gg |t|$ . We then replace the four-level model in Eq. (9) by a two-level model with the effective level positions

$$\varepsilon_1^{\text{eff}} = \varepsilon_1 + \varepsilon_{b1}; \quad \varepsilon_2^{\text{eff}} = \varepsilon_2 + \varepsilon_{b2} \quad (14)$$

To test this, we now solve the full model exactly. We introduce a complete basis set

$$\begin{aligned} |\tilde{1}\rangle &= \psi_1^\dagger \psi_{b1}^\dagger |0\rangle \\ |\tilde{2}\rangle &= \psi_2^\dagger \psi_{b2}^\dagger |0\rangle \\ |\tilde{3}\rangle &= \psi_1^\dagger \psi_{a1}^\dagger |0\rangle \\ |\tilde{4}\rangle &= \psi_2^\dagger \psi_{a2}^\dagger |0\rangle, \end{aligned} \quad (15)$$

where we have chosen the basis set so that only the first two states are relevant if the assumptions above are correct. We now calculate the resolvent operator [14]

$$(z - H)^{-1} = \begin{pmatrix} z - \varepsilon_1 - \varepsilon_{b1} & -t \cos\phi & 0 & t \sin\phi \\ -t \cos\phi & z - \varepsilon_2 - \varepsilon_{b2} & -t \sin\phi & 0 \\ 0 & -t \sin\phi & z - \varepsilon_1 - \varepsilon_{a1} & -t \cos\phi \\ t \sin\phi & 0 & -t \cos\phi & z - \varepsilon_2 - \varepsilon_{a2} \end{pmatrix}^{-1}. \quad (16)$$

We now focus on the upper left  $2 \times 2$  corner and use Löwdin folding [12] to project out the two high-lying states. For instance, the 11 element takes the form

$$\tilde{H}_{11} = \varepsilon_1 + \varepsilon_{b1} + \frac{t^2 (z - \varepsilon_1 - \varepsilon_{a1}) \sin^2\phi}{(z - \varepsilon_1 - \varepsilon_{a1})(z - \varepsilon_2 - \varepsilon_{a2}) - t^2 \cos^2\phi}. \quad (17)$$

For simplicity, we put  $\varepsilon_1 = \varepsilon_2$  and assume that the term  $t^2 \cos^2\phi$  in the denominator can be neglected. Putting  $z \approx \varepsilon_1 + \varepsilon_{b1}$ , we then find that the correction term in Eq. (17) is of the order  $t(t/V)(U_{sd}/V)^2$ . If  $|V| \gg |t|$  and  $|V| \gg U_{sd}$ , it is indeed justified to neglect the correction term. We then find that the level positions difference,  $\varepsilon_1^{\text{eff}} - \varepsilon_2^{\text{eff}}$ , have corrections to zeroth order in  $(1/V)$ , due to  $\varepsilon_{b1}$  and  $\varepsilon_{b2}$ . These corrections are included in our intuitive approach above.

$V$	$\varepsilon_2^{\text{eff}} - \varepsilon_1^{\text{eff}}$	$U^{\text{eff}}$	$E_0 + 2V$		$n_2$		$\chi$	
			Renorm.	Exact	Renorm.	Exact	Renorm.	Exact
1.0	1.17	3.18	-1.05	-0.95	0.380	0.364	0.314	0.312
1.5	1.39	3.21	-0.97	-0.90	0.339	0.326	0.266	0.262
2.0	1.53	3.29	-0.92	-0.88	0.317	0.307	0.240	0.237
3.0	1.68	3.44	-0.87	-0.85	0.292	0.287	0.214	0.213
4.0	1.75	3.55	-0.85	-0.84	0.280	0.277	0.202	0.201
6.0	1.83	3.68	-0.83	-0.82	0.268	0.267	0.190	0.190
10.0	1.90	3.80	-0.81	-0.81	0.259	0.258	0.181	0.181
20.0	1.95	3.90	-0.80	-0.80	0.252	0.252	0.174	0.174

**Table 1:** Ground-state energy  $E_0$ , occupancy  $n_2$  of level 2 and susceptibility  $\chi$  of the spin-degenerate model (9). The parameters are  $\varepsilon_1 = \varepsilon_2 = \varepsilon_3 = \varepsilon_4 = 0$ ,  $t = 1$ ,  $U_{dd} = 4$  and  $U_{sd} = 2$ .

Then there is a second order correction to the hopping integral due to  $\cos \phi$ . This correction is due to the fact that the electron in the space 3+4 cannot completely follow the electron in space 1+2 in the optimum way. This correction is usually neglected.

We now turn to the same model with spin degeneracy. The exact solution can then be obtained from a  $16 \times 16$  matrix. In this case the analytical calculation is too complicated to illustrate what happens, and we focus on a numerical calculation. We first calculate the energy  $E(n_2)$  of the 3+4 space as a function of the occupancy of level 2. We then obtain

$$\begin{aligned}
\varepsilon_1^{\text{eff}} &= \varepsilon_1 + E(0) \\
\varepsilon_2^{\text{eff}} &= \varepsilon_2 + E(1) \\
U^{\text{eff}} &= E(2) + E(0) - 2E(1)
\end{aligned} \tag{18}$$

in analogy with the spinless case. We then calculate the ground-state energy,  $E_0$ , the occupancy  $n_2$  of level 2 and the spin susceptibility  $\chi = -\partial^2 E_0(H)/\partial H^2$ , where the model couples to an external magnetic field via the term  $-H(n_{2\uparrow} - n_{2\downarrow})$ . The results are shown in Table 1. We have added a contribution  $2V$  to the total energy  $E_0$ , since there would have been a trivial contribution  $-2V$  if there had been no interaction between spaces 1+2 and 3+4. As expected, the agreement between the approximate (Renorm.) and exact results improves as  $|V|$  is increased. However, the agreement is surprisingly good even for  $V = t$ .

### 3 Effective Coulomb interaction

The essential point of the model from the previous section is that we can distinguish between two types of electrons, “slow” electrons (space 1+2) and “fast” electrons (space 3+4), in the following referred to as “localized” and “delocalized”. The idea is that the delocalized electrons are assumed to adjust in an optimum way to the movements of the localized electrons. We can then estimate effective parameters in a similar way as in the previous section. For each system we then have to decide which electrons we consider localized and include explicitly in the model

System	Localized	Delocalized
4 <i>f</i> compounds	4 <i>f</i>	5 <i>d</i>
3 <i>d</i> compounds	3 <i>d</i>	4 <i>s</i> , 4 <i>p</i>

**Table 2:** "Slow" ("localized") and "fast" ("delocalized") electrons for 3*d* and 4*f* compounds.

and which are delocalized and only included implicitly as a renormalization of the parameters. This is illustrated in Table 2. For 4*f* compounds the 4*f* DFT band width is about 1/10 of the 5*d* band-width, and we may reasonably talk about two types of electrons. For 3*d* compounds this distinction is much less clear cut.

### 3.1 Perfect screening

We now focus on the calculation of an effective Coulomb integral  $U^{\text{eff}}$  as an essential model parameter. We apply the approach of the previous section to a real system. For that reason, we need to know how the energy of the system varies with the occupancy of, e.g., a 3*d* or 4*f* level, Eq. (18). Herring [15] estimated these energies using atomic data, assuming that any change in the number of localized electrons on an atom is compensated by the opposite change in the number of delocalized electrons on the same atom. For a 3*d* metal this can be written as

$$U = E(3d^{n+1}4s^0) + E(3d^{n-1}4s^2) - 2E(3d^n4s^1), \quad (19)$$

where  $E(3d^n4s^m)$  is the energy of an atom (ion) with  $n$  3*d* electrons and  $m$  4*s* electrons. In this approach it is assumed that the variation in the number of 3*d* electrons is perfectly screened by a change in the number of 4*s* electrons. We refer to this as "perfect screening".

A similar method was used by Cox *et al.* [16] who studied transition metals and Herbst *et al.* [17] who studied the rare earths. They performed Hartree-Fock calculations for renormalized atoms with Wigner-Seitz boundary conditions.

### 3.2 Constrained density functional formalism

Dederichs *et al.* [18] calculated  $U$  using a constrained density functional formalism. The functional for a 3*d* compound is written as

$$E[n_{3d}^i] = F[n] + \int d^3r V_{\text{ext}}(\mathbf{r})n(\mathbf{r}) + \mu \left( \int d^3r n(\mathbf{r}) - N \right) + \mu_{3d}^i \left( \int d^3r n_{3d}^i(\mathbf{r}) - n_{3d}^i \right). \quad (20)$$

Here  $F[n]$  describes the kinetic and potential energy of the system,  $V_{\text{ext}}(\mathbf{r})$  is an external potential,  $\mu$  is the chemical potential and  $\mu_{3d}^i$  is a Lagrange parameter.  $n_{3d}^i$  is the number of localized electrons on site  $i$ , referred to as the central site in the following. A stationary point of the energy functional to density variations is searched

$$0 = \frac{\partial F}{\partial n} + V_{\text{ext}}(\mathbf{r}) + \mu + \mu_{3d}^i P_{3d}^i, \quad (21)$$

where  $P_{3d}^i$  is a projection operator acting on the localized electrons. From this a new Kohn-Sham equation can be derived, where  $\mu_{3d}^i$  enters as an additional nonlocal potential acting only on the localized electrons.  $\mu_{3d}^i$  is varied until the prescribed number of  $3d$  electrons is obtained. This requires a definition of localized electrons. For instance, in methods based on an expansion in spherical waves in a region around each nucleus a natural definition can be introduced. This way an effective  $U^{\text{eff}}$  is calculated, using a formula equivalent to Eq. (18).

In the approach above,  $U^{\text{eff}}$  contains a change of the kinetic energy of the electrons included explicitly in the model. This contribution needs to be subtracted. Hybertson *et al.* [19] did this by considering the model Hamiltonian in which  $U^{\text{eff}}$  will be used, e.g.,

$$H = \sum_{ij\sigma} t_{ij} \psi_{i\sigma}^\dagger \psi_{j\sigma} + \sum_i U^{\text{eff}} n_{i\uparrow} n_{i\downarrow}, \quad (22)$$

where  $t_{ij}$  are hopping integrals. This model is then solved in a constrained mean-field theory to simulate the constrained density functional approach. The energy as a function of the constrained occupancies is calculated, and  $U^{\text{eff}}$  is varied until the constrained DFT result is reproduced. We refer to this as cLDA. Cococcioni and Giroconcoli [20] used a similar approach. An alternative approach was used by McMahan *et al.* [21] and by Gunnarsson *et al.* [22]. They performed a band structure calculation with a large unit cell [21–23]. Then the hopping integrals from the orbital with localized electrons is cut off for the central atom in the unit cell. Then the occupation of the orbital can be trivially varied without a variation of the kinetic energy for hopping in and out of the orbital, since this energy is zero. Double-counting is also explicitly avoided, contrary to claims elsewhere [24]. This method is referred to as “cut off” LDA. In a different method, the hopping between the localized orbitals and the delocalized orbitals was cut on all sites, not only on the central site [28].

### 3.3 Constrained RPA

A different approach was taken by Aryasetiawan *et al.* [25]. They calculated the Coulomb interaction using a constrained random phase screening. In the random phase approximation (RPA) the polarizability is written as

$$P(\mathbf{r}, \mathbf{r}'; \omega) = \sum_i^{\text{occ}} \sum_j^{\text{unocc}} \psi_i(\mathbf{r}) \psi_i^*(\mathbf{r}') \psi_j^*(\mathbf{r}) \psi_j(\mathbf{r}') \left( \frac{1}{\omega - \varepsilon_j + \varepsilon_i + i0^+} - \frac{1}{\omega + \varepsilon_j - \varepsilon_i - i0^+} \right),$$

where  $\psi_i(\mathbf{r})$  and  $\varepsilon_i$  are one-particle eigenfunctions and eigenvalues. Calculating the effective Coulomb interaction by using this screening would be incorrect, since it would involve double-counting. The Hubbard model explicitly allows localized electrons to screen the interaction between localized electrons, and the use of Eq. (23) would then lead to double counting. Aryasetiawan *et al.* [25] therefore excluded contributions to Eq. (23) where both  $i$  and  $j$  stand for Bloch states containing mainly localized states. For a transition metal compound they then excluded states within an energy window where the states are mainly of  $3d$  character and for a rare earth compound a window where the states are mainly of  $4f$  character. The definition of the energy window involves uncertainties [25]. This method is referred to as cRPA.

Unrenormalized ( $F^0$ )	21.4 eV
Relaxation of 3d orbital	-5.2 eV
Relaxation of 4s, 4p orbitals	-2.2 eV
Relaxation core, XC effects	-1.2 eV
Atomic $U$	12.8 eV

**Table 3:** Contribution to  $U$  for a free Mn atom with the configuration  $3d^{5.1}4s^{0.64}4p^{0.70}$ . This corresponds to the configuration for Mn in CdTe.

On-site relaxation	15.4 eV
Charge transfer to Mn	-7.6 eV
Charge transfer to n.n. ligand	-0.4 eV
Solid state $U$	7.4 eV

**Table 4:** Contribution to  $U$  for a Mn impurity in CdTe.

### 3.4 Screening and breathing

The definition of  $U$  can be approximately rewritten as

$$U = E(n+1) + E(n-1) - 2E(n) \approx \frac{\delta\varepsilon}{\delta n}, \quad (23)$$

where  $E(n)$  is the energy of the system with  $n$  localized electrons and  $\varepsilon$  is the energy eigenvalue of the localized orbital and  $n$  is the occupancy. If the system were not allowed to relax, this would lead to  $U = F$ , where  $F$ , given in Eq. (2), is the direct Coulomb integral of the orbital. In reality, the charge density relaxes and the corresponding change in the electrostatic potential acts back on the orbital eigenvalue, reducing the shift as  $n$  is varied and leading to a renormalized  $U$ . We can illustrate this for the case of a Mn impurity in CdTe [26]. First a free Mn atom is studied (Table 3). The spherical part  $F_{3d,3d}^0$  of the direct Coulomb integral is large, 21 eV. The main renormalizing process is a breathing of the 3d orbital, where the orbital expands as the 3d occupancy is increased [26, 29]. This reduces  $U$  by about 5 eV. Breathing of the 4s, 4p and core orbitals contribute less. The net result is a reduction of  $U$  from about 21 eV to about 13 eV. In the solid there are similar breathing effects, reducing  $U$  to about 15 eV (see Table 4). However, now there is additional charge transfer from the surrounding to the Mn atom, reducing the  $U$  by almost 8 eV. Charge transfer to near neighbors (n.n.) plays a smaller role. The result is reduction of  $U$  to about 7 eV according to this calculation.

The breathing effect can also be understood from Slater's rules [30]. According to these rules, the effective nuclear charge for a 3d orbital is  $Z^* = Z - 18 - 0.35(n_{3d} - 1)$ , where  $Z$  is the true nuclear charge and  $n_{3d}$  is the 3d occupancy. This illustrates how the effective nuclear charge is reduced and the orbital expands as  $n_{3d}$  is increased. According to Slater's rules, the occupancy of the 4s and 4p orbitals do not influence  $Z^*$  for the 3d orbital. This then suggests that the charge transfer in the solid to 4s and 4p should not influence breathing very much. This is also supported by a comparison of Tables 3 and 4.

System	cLDA	“cut-off”	cRPA	“perfect screening”	Exp
Fe	2.2 [20]	6 [23]	4 [25]	2.7 [16]	2 [31,32]
Ce	4.5 [20]	6 [23]	3.2-3.3 [25]	5 [17]	5-7 [35]

**Table 5:** Results for  $U$  for Fe as an example of a 3d metal and Ce illustrating a 4f metal.

### 3.5 Results

We now consider results obtained using the methods above for 3d and 4f metals. Specifically, we consider Fe and Ce as examples of 3d and 4f metals. The results are shown in Table 5. “Perfect screening” provides a rather good estimate for both Fe and Ce. The “cut-off” method gives a substantially too large  $U$  for Fe. It was found [23] that only about half the screening charge is on the Fe atom, as one would expect from the energetics of the screening process [23]. It is then to be expected that  $U$  is substantially larger than the “perfect screening” result. cLDA gives a very good result compared with experiment, and actually somewhat smaller than “perfect screening”. It is not clear why this result is so different from the “cut-off” method, and it would be interesting to study the screening in cLDA. The  $U$  in cRPA is a bit too large. Interestingly, the “cut-off” method gives a good estimate of  $U$  towards the end of the 3d series, e.g., for the cuprates [34].

For Ce “perfect screening” provides a fairly accurate estimate of  $U$ . The “cut off” method gives only a slightly larger  $U$ , in good agreement with experiment. In this case it is found that the screening charge on Ce is approximately unity [23], so it is not surprising that there is rather good agreement with “perfect screening”. cLDA gives a  $U$  slightly smaller than “perfect screening” and  $U$  in cRPA is substantially smaller. It is not clear why cRPA implies such an effective screening and gives a  $U$  that is only roughly half the experimental estimate.

## 4 Neglected renormalizations

In this section we discuss two renormalizations of parameters, which are usually neglected. The purpose is not to argue that these effects should be included. This could be done, but it would result in more parameters and the results would probably be less transparent. The purpose is rather to illustrate that the parameters of effective models contain complicated renormalizations, and that *ab initio* estimates of such parameters may neglect several such effects. The purpose is also to show that if we insist on a rather simple model, which is advocated here, the effective parameters may actually be different for different properties.

### 4.1 Configuration dependence of hopping integrals

We already discussed in Sec. 3.4 that there is a substantial breathing of the localized orbital when the occupancy is changed. This changes the hopping integral into this orbital. In the LMTO method [36], used here, the hopping integral  $V$  is related to a potential parameter  $\tilde{\Delta}$ ,

$$V^2 \sim \tilde{\Delta} \approx \frac{s}{2} [\phi_l(C, s)]^2, \quad (24)$$

$n_l$	$n_c$	Mn	Ce	U
$n_l^0 - 1$	$n_c^0$	51	8	72
$n_l^0$	$n_c^0$	85	19	91
$n_l^0 + 1$	$n_c^0$	129	38	112
$n_l^0$	$n_c^0 - 1$	40	5	53
$n_l^0 + 1$	$n_c^0 - 1$	67	11	69

**Table 6:** Potential parameter  $\tilde{\Delta}$  for different configurations of Mn, Ce and U in non-spin-polarized calculations. The localized orbital is 3d (Mn), 4f (Ce) and 5f (U), and we consider a core hole in the 1s (Mn), 3d (Ce) and 4f (U) orbital. The occupancy of the localized and core orbital is  $n_l$  and  $n_c$ , respectively. We introduce  $n_l^0$ , which is 5 (Mn), 1 (Ce) and 3 (U) and  $n_c^0$  which is 2 (Mn), 10 (Ce) and 14 (U). All energies are in mRy.

where  $\phi_l(C, s)$  is the value of the localized orbital at the Wigner-Seitz radius  $s$ . The localized orbital with the angular momentum  $l$  is solved for an energy  $C$ , which gives the logarithmic derivative  $-l - 1$  at  $s$ . The value of  $\tilde{\Delta}$  is shown in Table 6 for a few metals with and without a core hole [27]. The table illustrates the strong dependence of the hopping on the configuration used to calculate  $\tilde{\Delta}$ . For instance, if we want to describe how a host electron hops into a Ce atom, should we then use the initial configuration or the final configuration to calculate  $\tilde{\Delta}$  or should we use an average? Table 6 shows that the difference could be even as much as a factor of two.

To address this issue, we temporarily introduce an impurity model with two orbitals [27]

$$\begin{aligned}\varphi_l^0 &\equiv \varphi_l(r, n_l^0) \\ \varphi_l^1 &\equiv A \frac{\partial}{\partial n_l} \varphi_l(r, n_l) |_{n_l=n_l^0},\end{aligned}\tag{25}$$

where  $A$  is chosen so that  $\phi_l^1$  is normalized. By forming linear combinations of  $\varphi_l^0$  and  $\varphi_l^1$ , we can obtain an appropriate orbital for different occupancies, i.e., describing breathing. In, for instance, an Anderson impurity model we then introduce a term leading to transitions between these two orbitals

$$\tilde{U} \sum_{m\sigma} (\psi_{1m\sigma}^\dagger \psi_{0m\sigma} + \text{H.c.}) (n_0 + n_1 - n_l^0),\tag{26}$$

where  $n_i = \sum_{m\sigma} n_{im\sigma}$ . If the occupancy of the two levels adds up to  $n_l^0$ , the orbital  $\varphi_l^0$  is appropriate and there is no mixing of the orbital  $\varphi_l^1$ . For any other occupancy, transitions to  $\varphi_l^1$  are induced and the system has the freedom to adjust to the occupancy. For Mn in CdTe we find that  $\tilde{U} = 0.16$  Ry. The energies of the two orbitals are quite different,  $\varepsilon_0 = -0.45$  Ry and  $\varepsilon_1 = 1.68$  Ry. The model then tends to have two sets of states, one set at  $\varepsilon_0$  and one set at  $\varepsilon_1$ . We can then project out all high-lying states, having a substantial weight in  $\varphi_l^1$ . The result is then that we recover the normal Anderson impurity model, with just one localized orbital. But in this process the hopping matrix elements are modified. Since the mixing matrix element  $\tilde{U}/(\varepsilon_1 - \varepsilon_0) = 0.08 \ll 1$ , this approach should be rather accurate.

We can then answer the question of how to calculate these elements. Let us consider a host electron hopping into a configuration with  $n_l$  localized electrons, resulting in a configuration

with  $n_l + 1$  localized electrons. The projection procedure then shows that the matrix element should be calculated using  $n_l + 1$  electrons, i.e., the end configuration [27]. For  $n_l = 0$  this is easy to understand. In the initial state there is no localized electron and the extent of the localized wave function then plays no role. It is then natural that it is the wave function in the final configuration that matters. In a similar way it is the initial configuration that matters when an electron hops out of the localized orbital.

We then should be using different hopping integrals for different experiments. For Ce compounds, for instance,  $f^0 - f^1$ -hopping is particularly important for valence photoemission, and we would use  $n_l = 1$  for calculating these hopping matrix elements. For inverse photoemission, we are often interested in the relative weights of the  $f^1$  and  $f^2$  peaks. We then need to distinguish between the calculation of the ground-state and the calculation of the final states, resulting from the inverse photoemission process. In the ground-state calculation the important matrix elements would be calculated for  $n_l = 1$  and in the final state for  $n_l = 2$ . For core level spectroscopies we should in addition include a core hole for the calculation of matrix elements for the final states but not for the ground-state.

As argued above, this would lead to a complicated model. It seems questionable if the possible additional gain in physics would justify such a complicated model with additional parameters. However, the example illustrates one source of uncertainty in models with configuration independent hopping parameters. It also illustrates how parameters can be different for different experiments.

## 4.2 Many-body renormalization of hopping integrals

In Secs. 2.2 and 3 we discussed how the effective level energies and Coulomb integrals can be obtained by letting delocalized electrons adjust to the movements of localized electrons. This approach, however, raises questions about other many-body effects. One issue is the Anderson orthogonality catastrophe [37]. Consider the case when delocalized electrons interact with a (truly) localized electron via the Coulomb interaction. Let us then change the occupancy of the localized level by one and let  $|0\rangle$  and  $|1\rangle$  be the lowest states of the delocalized electrons in the presence of 0 or 1 localized electrons, respectively. Then  $\langle 0|1\rangle = 0$  for an infinite system [37]. One might then think that the hopping integrals should be reduced by such effects. When a delocalized electron hops into a localized level, all the other electrons would adjust their wave functions to the new potential. Then one might expect that the overlap  $\langle 0|1\rangle = 0$  enters the effective hopping integral. This is, however, not the appropriate comparison. Anderson's orthogonality catastrophe refers to the case when the localized electron is removed from the system. Here it hops into or out of delocalized states. The appropriate comparison is then X-ray absorption (XAS) or X-ray emission (XES). In addition to the Anderson effect there is then an exciton like effect, transferring spectral weight towards the Fermi energy. For instance, the XES spectrum looks like

$$S(\omega) \sim \left( \frac{\tilde{\omega}}{\omega - \omega_0} \right)^\alpha \Theta(\omega - \omega_0), \quad (27)$$

$\varepsilon_d$	$U_{sd}$	$-\Delta E$					$n_d$					$\varepsilon_d^{\text{calc}}$	$\varepsilon_d^{\text{fit}}$	$t_{\text{off}}^{\text{fit}}$
		Ex.	Ren.	Unre.	Fit	XAS	Ex.	Ren.	Unre.	Fit	XAS			
-1.5	1	1.33	1.28	1.66	1.33	1.31	0.89	0.91	0.94	0.89	0.89	-1.09	-1.09	1.12
-1.5	2	1.12	1.02	1.66	1.12	1.08	0.82	0.87	0.94	0.83	0.81	-0.79	-0.81	1.18
-1.5	3	0.98	0.83	1.66	0.99	0.94	0.76	0.81	0.94	0.78	0.74	-0.57	-0.64	1.21
-1.5	5	0.83	0.62	1.66	0.88	0.78	0.66	0.70	0.94	0.69	0.62	-0.29	-0.41	1.30
-1.0	3	0.64	0.48	1.20	0.69	0.62	0.57	0.55	0.90	0.55	0.53	-0.07	-0.09	1.31
-0.5	3	0.42	0.29	0.78	0.44	0.41	0.33	0.24	0.79	0.31	0.31	0.43	0.36	1.22
0.0	3	0.29	0.21	0.44	0.30	0.29	0.18	0.11	0.50	0.17	0.17	0.93	0.76	1.15
10	3	.043	.040	.043	.044	.043	.004	.003	.004	.004	.004	10.9	10.1	1.00

**Table 7:** Energy lowering  $\Delta E$  and occupancy of the  $d$  level  $n_d$  in the exact calculation (“Ex.”) compared with results of calculations for the model (28) with  $U_{sd} = 0$ . The unrenormalized  $d$  level position was used for “Unre.” and the calculated renormalized position for “Ren.” and “XAS”. For “XAS” the effective hopping integral was renormalized [Eq. (29)] and for “Fit” both the level position and the hopping were adjusted to obtain the best agreement with the exact results. The parameters are  $t = 1$ ,  $B = 5$ ,  $N = 17$  and  $N_{el} = 9$ .

where  $\tilde{\omega}$  is a typical energy and  $\omega_0$  is the threshold energy. The exponent  $\alpha$  is positive and determined by the phase shift due to the Coulomb interaction between localized and delocalized electrons. From Eq. (27) we might then expect hopping integrals for states close to the Fermi energy to be enhanced. This would then in particular influence thermodynamic properties.

To check these ideas we have considered the spinless model [38]

$$H = \sum_{k=1}^N \varepsilon_k n_k + \varepsilon_d n_d + \frac{t}{\sqrt{N}} \sum_{k=1}^N (\psi_k^\dagger \psi_d + \text{H.c.}) + \frac{U_{sd}}{N} \sum_{k=1}^N \sum_{l=1}^N \psi_k^\dagger \psi_l n_d, \quad (28)$$

where we have introduced  $N$  delocalized states with the energies  $\varepsilon_k$  and a localized state with the energy  $\varepsilon_d$ . There is a hopping integral  $t$ , connecting the localized and delocalized states. When the localized level is occupied the delocalized electrons feel a scattering potential  $U_{sd}$ . The delocalized levels are equally spaced over an energy  $2B$ .

This model can be solved using exact diagonalization for finite  $N$  [38]. We have used  $N = 17$  and the number of electrons  $N_{el} = 9$ . Although this is far from an infinite system, Anderson’s orthogonality catastrophe already has an effect. For  $B = 5$ ,  $\varepsilon_d = -1.5$  and  $U_{sd} = 5$ , the overlap between the lowest states of delocalized electrons in the presence or absence of a localized electron is  $0.85 < 1$ . We then calculate the energy lowering  $\Delta E = E_0 - \sum_k' \varepsilon_k$ , where  $E_0$  is the ground-state energy and the sum goes over the  $N_{el}$  lowest states. We have also calculated the  $3d$  occupancy,  $n_d$  and the charge susceptibility  $\chi_c = -\partial n_d / \partial \varepsilon_d$ . The results are shown in Table 7 and 8.

We compare the exact results with several approximations [38]. In all these calculations  $U_{sd}$  was put to zero and its effects were approximately included via renormalized parameters. The column “Ren.” shows results where  $\varepsilon_d$  was replaced by  $\varepsilon_d^{\text{calc}} = \tilde{E}_0(1) - \tilde{E}_0(0)$ . Here  $\tilde{E}_0(n_d)$  is the energy of the model as a function of the occupancy  $n_d$ . In this calculation the hopping to the

$\varepsilon_d$	$U_{sd}$	$\chi_c$					$\varepsilon_d^{\text{calc}}$	$\varepsilon_d^{\text{fit}}$	$t_{\text{eff}}^{\text{fit}}$
		Ex.	Ren.	Unre.	Fit	XAS			
-1.5	1	0.12	0.10	0.05	0.12	0.13	-1.09	-1.09	1.12
-1.5	2	0.20	0.19	0.05	0.20	0.23	-0.79	-0.81	1.18
-1.5	3	0.27	0.30	0.05	0.28	0.32	-0.57	-0.64	1.21
-1.5	5	0.36	0.55	0.05	0.38	0.40	-0.29	-0.41	1.30
-1.0	3	0.47	0.74	0.12	0.50	0.47	-0.07	-0.09	1.31
-0.5	3	0.41	0.41	0.35	0.43	0.37	0.43	0.36	1.22
0.0	3	0.21	0.14	0.75	0.22	0.19	0.93	0.76	1.15
10	3	.0006	.0005	.0006	.0006	.0006	10.9	10.1	1.00

**Table 8:** Same as Table 7 but for calculating  $\chi$ .

localized level was cut to avoid double-counting. The Table also shows results for unrenormalized parameters (“Unre.”). We then treated the  $\varepsilon_d^{\text{fit}}$  and  $t_{\text{eff}}^{\text{fit}}$  as fitting parameters, and adjusted these parameters to obtain the best possible agreement (“Fit”) with the exact results. Finally we have performed calculations where the hopping matrix element to a level  $\varepsilon_k$

$$(t_{\text{eff}}(\varepsilon_k))^2 = t^2 S(|\varepsilon_k - \varepsilon_F + \omega_0|), \quad (29)$$

was related to the X-ray absorption or emission spectra.  $t_{\text{eff}}(\varepsilon_k)^2$ , summed over all states, is unrenormalized, but the hopping parameters to states close to the Fermi energy,  $\varepsilon_F$ , are enhanced at the cost of hopping to the band edges. In calculations with  $t_{\text{eff}}(\varepsilon_k)$  we used the renormalized level position  $\varepsilon_d^{\text{calc}}$ .

We first compare the exact results with the unrenormalized and renormalized results. The renormalization improves the agreement with the exact results substantially. For most parameter sets the agreement is relatively good. For  $U_{sd}$  large and for  $|\varepsilon_d|$  rather small, there are still substantial deviations. “XAS” shows the results when the hopping is renormalized as well, using Eq. (29). There is then a substantial additional improvement, and the agreement is now generally rather good. Finally, we have treated both the hopping and the level position as adjustable parameters. This gives only a marginal improvement and sometimes the results are even worse. This is remarkable, since the  $d$ -level position is now also a fit parameter and  $\varepsilon_d^{\text{calc}}$  is sometimes rather different from  $\varepsilon_d^{\text{fit}}$ . On the other hand, hopping is energy-dependent, and “XAS” presumably describes this better than “Fit”. This suggests that Eq. (29) gives a quite good renormalization.

In the case of Ce the delocalized states are primarily of  $5d$  character. According to the Friedel sum rule we can then estimate the phase shift as  $\delta \sim \pi/10$ . This then gives a singularity index of the order  $\alpha \sim 0.1$ . For thermodynamic properties we may then expect an enhancement of the order of  $(\tilde{\omega}/T_K)^{0.1}$ , where  $T_K$  is the Kondo temperature. For, e.g., CeCu<sub>2</sub>Si<sub>2</sub>  $T_K = 0.001$  eV, and  $t^2$  may then be enhanced by a factor of two, if we assume  $\tilde{\omega} \sim 1$  eV. As discussed above, we do not advocate including these effects explicitly in a model. However, one should be aware that thermodynamic and spectroscopic properties may be renormalized differently.

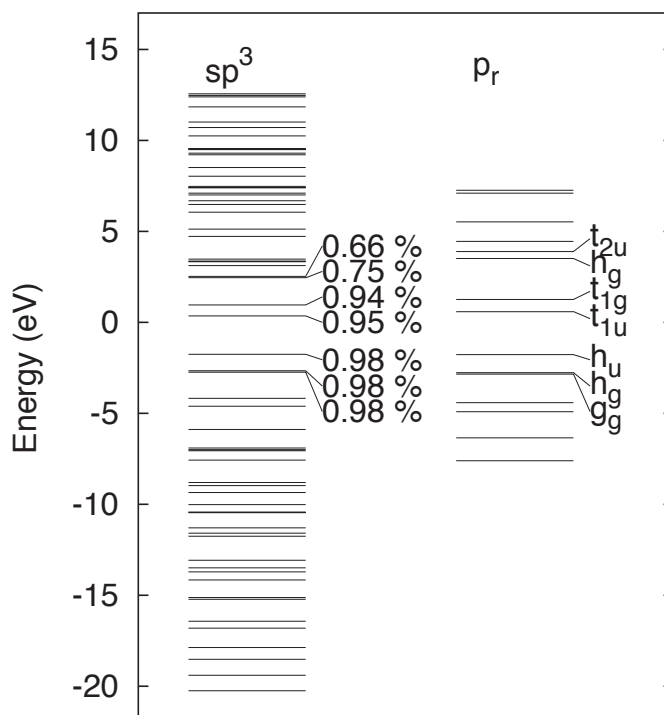


**Fig. 3:** Levels of the C<sub>60</sub> molecule. The left-hand part shows the levels obtained by using a basis of one 2s and three 2p orbitals per carbon atom ( $sp^3$ ). The right-hand part shows the levels obtained by using just one radial 2p orbital per atom ( $2p_r$ ). The numbers give the amount of radial 2p character ( $2p_r$ ) in the full calculation (after Ref. [39]).

## 5 Fullerenes

In this section we discuss the parameters for a molecular solid. As an example we use fullerenes [39]. Similar work has been done for TTF-TCNQ [40].

### 5.1 Hopping

The important levels in a C<sub>60</sub> molecule can be described in a tight-binding picture including a 2s and three 2p orbitals on each of the 60 C atoms. The corresponding molecular levels are shown in Fig. 3. The molecule forms approximate  $sp^2$  hybrids on each C atom which point towards the neighboring C atoms and radial orbitals  $p_r$  pointing out of the molecule. The former orbitals interact strongly and form bonding and antibonding molecular orbitals at the lower and upper end of the spectrum, respectively. The  $p_r$  orbitals interact much less and form molecular orbitals in the middle of the spectrum. The figure illustrates that these molecular orbitals can be described rather well using only the  $p_r$  orbitals. In the neutral molecule all orbitals up to and including the  $h_u$  orbital are filled.

C<sub>60</sub> molecules condense to a solid of rather weakly bound molecules. Thus the distance ( $\sim 3$  Å) between the closest C atoms on two neighboring molecules is much larger than the distance ( $\sim 1.4$  Å) between two C atoms on the same C<sub>60</sub> molecule. The molecular levels then essentially

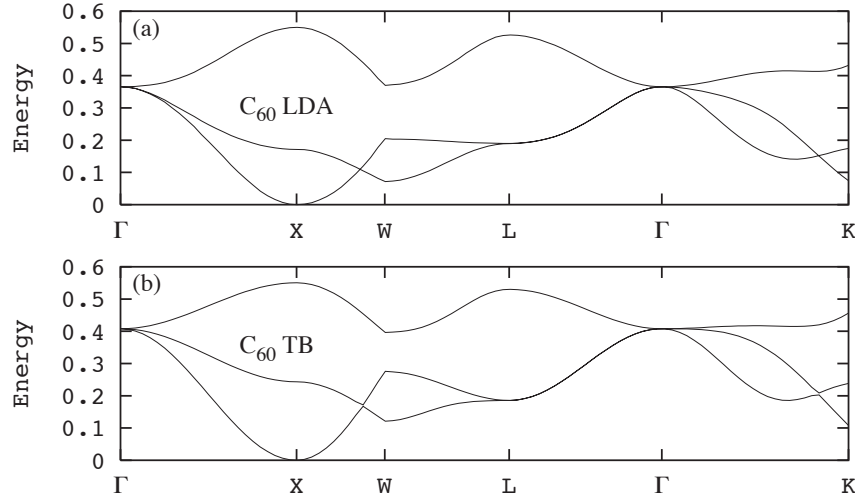


**Fig. 4:** Band structure for a  $C_{60}$  solid in the  $Fm\bar{3}$  structure (a) according to an *ab initio* LDA and (b) according to a TB calculation (after Gunnarsson *et al.* [43]).

preserve their identity in the solid, but the discrete molecular levels are broadened to narrow, essentially non-overlapping bands. The alkali-doped fullerenes are of particular interest. In these systems the  $t_{1u}$  band is partly filled. Therefore the three-fold degenerate  $t_{1u}$  molecular level is particularly interesting.

The band structure can be described in a tight-binding (TB) scheme. We first form a molecular orbital corresponding to the  $t_{1u}$  level. The hopping between the molecules is described by hopping integrals  $V_{pp\sigma}$  and  $V_{pp\pi}$  corresponding to hopping between orbitals pointing directly towards each other or orbitals pointing perpendicular to the connecting line of the centers. Following Harrison [41], we assume that the ratio of the  $\pi$ - and  $\sigma$ -integrals is  $-1/4$ . Then

$$V_{pp\sigma} = v_{\sigma} \frac{R}{R_0} e^{-\lambda(R-R_0)}; \quad \frac{V_{pp\pi}}{V_{pp\sigma}} = -\frac{1}{4} \quad R_0 = 3.1 \text{ \AA}, \quad (30)$$

where  $R$  is the separation of the carbon atoms. The prefactor  $R$  has been included to simulate the  $r$ -dependence of a  $2p$  orbital as described by Slater's rules [30]. The overall hopping strength, determined by  $v_{\sigma}$ , is adjusted to the band-width in a band structure calculation, and the decay length  $\lambda$  is determined from the dependence of the band width on the lattice parameter. Here we use the parameters [42, 43]

$$\lambda = 1.98 \text{ \AA}^{-1} \text{ and } v_{\sigma} = 0.917 \text{ eV}. \quad (31)$$

The resulting TB band structure is compared with an *ab initio* band structure calculation in Fig. 4. The agreement is quite good. The resulting band structure  $\varepsilon_{\mathbf{k}}$  has a simple parameterization [42, 44]. The dominating hopping between two molecules in this structure is given by two equivalent hopping integrals, with all other hopping integrals being substantially smaller. Effectively, we have therefore adjusted this parameter, requiring that the TB band width should agree with the LDA band width. The shape of the band structure in Fig. 4 is therefore primarily determined by the geometry of the  $C_{60}$  molecule and by the relative positions and orientations of the  $C_{60}$  molecules in the  $Fm\bar{3}$  symmetry.

## 5.2 Coulomb interaction

We first consider the Coulomb integral  $U_0$  between two  $t_{1u}$ -electrons for a free  $C_{60}$  molecule. A very simple estimate is obtained by assuming that the charge density of the  $t_{1u}$  orbital forms a thin shell of charge on a sphere with the radius of the  $C_{60}$  molecule  $R \sim 3.5 \text{ \AA}$ . Then  $U_0 = 1/R \approx 4 \text{ eV}$ . This neglects that the orbitals breath when the occupancy is changed. To obtain a better estimate one can calculate how the  $t_{1u}$  eigenvalue changes with occupancy, using Eq. (23) and LDA. This leads to values of the order 2.7-3.0 eV [45–47].  $U_0$  for a free molecule can also be estimated from experimental results using

$$U_0 = I_p(C_{60}^-) - A(C_{60}^-) = E_0(2) + E_0(0) - 2E_0(1), \quad (32)$$

where  $E_0(n)$  is the energy of a  $C_{60}$  molecule with  $n$   $t_{1u}$  electrons. This leads to  $U_0 \sim 2.7 \text{ eV}$ , in fairly good agreement with theory [39, 48].

We next consider  $U$  for a  $C_{60}$  solid, following Antropov *et al.* [47].  $U$  is strongly screened by the polarization of the surrounding molecules. To describe this, we put the  $C_{60}$  molecules on an fcc lattice and assign a polarizability  $\alpha$  to each molecule. An electron is added to the central molecule, and the surrounding molecules are allowed to polarize in a self-consistent way. This polarization acts back on the electron and reduces the energy-increase of the  $t_{1u}$  level by an amount  $\delta U$ . The summation over neighboring molecules is extended until it is converged. The  $U$  for the solid is then

$$U = U_0 - \delta U. \quad (33)$$

The value of  $\alpha$  can be determined from the experimental value,  $\epsilon = 4.4$ , of the dielectric function [51]. Using the Clausius-Mossotti relation and the lattice parameter  $a = 14.04 \text{ \AA}$ , this leads to  $\alpha = 90 \text{ \AA}^3$ . *Ab initio* calculations using the density functional formalism give  $\alpha = 83 \text{ \AA}^3$  [46]. Using  $\alpha = 90 \text{ \AA}^3$ , Antropov *et al.* [47] found  $\delta U = 1.7 \text{ eV}$ . Together with  $U_0 = 2.7 \text{ eV}$ , this gives  $U = 1.0 \text{ eV}$ . These values of  $U$  do not include the metallic screening from the  $t_{1u}$  electrons in  $A_3C_{60}$  compounds, and they are appropriate for models where the metallic screening is treated explicitly when solving the corresponding model.

We next consider the nearest neighbor interaction  $V$ , which is obtained by calculating the increase of the energy of a  $t_{1u}$  orbital on a molecule 1 when an electron is added to a neighboring molecule 2. This leads to the result

$$V = 1/R_{nn} - \delta V, \quad (34)$$

where  $R_{nn}$  is the nearest neighbor separation and  $-\delta V$  is the lowering of the  $t_{1u}$  orbital on molecule 1 due to the polarization of the surrounding molecules when an electron is added to molecule 2. For  $a = 14.04 \text{ \AA}$ , Antropov *et al.* [47] estimated that  $\delta V = 1.12 \text{ eV}$ , resulting in  $V = 0.3 \text{ eV}$  for the polarizability  $\alpha = 90 \text{ \AA}^3$ . The same value  $V = 0.3 \text{ eV}$  was also obtained by Pederson and Quong [46]. We can see that  $U$  is indeed substantially larger than  $V$ , and that it is justified to focus on the effects of  $U$  at first.

$U$  can be estimated experimentally from Auger spectroscopy [49, 50]. A carbon  $1s$  electron is emitted in a photoemission process. This is followed by an Auger process, where a carbon

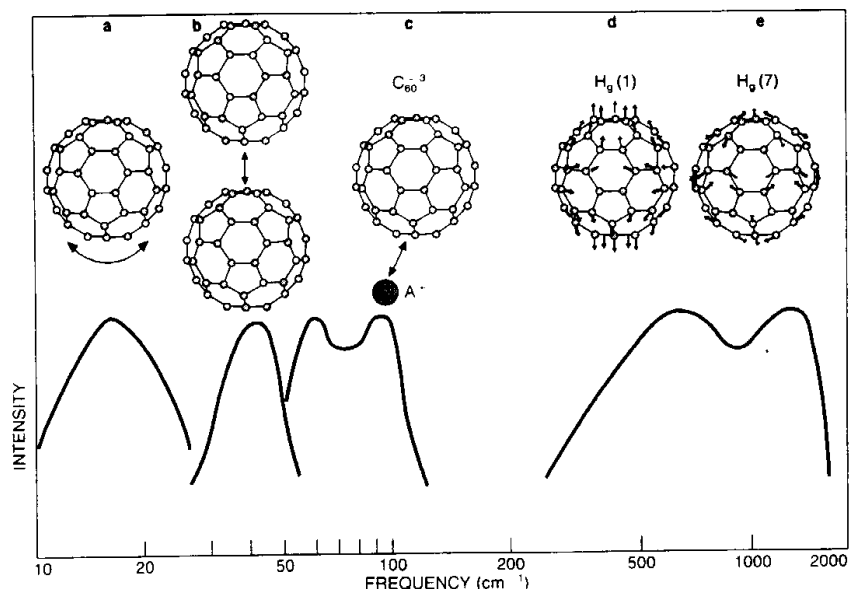


**Fig. 5:** Schematic representation of various phonons in  $A_3C_{60}$  compounds. The figure shows, from left to right, (a) librations, (b) intermolecular  $C_{60}$ - $C_{60}$  phonons, (c)  $A$ - $C_{60}$  phonons and (d)-(e) intramolecular  $H_g$  modes. The figure indicates the radial and tangential character of the low-lying and high-lying  $H_g$  modes, respectively (After Hebard [52]).

$2p$  electron falls down into the  $1s$  hole and another  $2p$  electron is emitted. For noninteracting electrons, the Auger spectrum is just the self-convolution of the photoemission spectrum. For the interacting system, the Auger spectrum is expected to be shifted due to the interaction of the two holes in the final state. Indeed, Lof *et al.* [49] found good agreement with the self-convoluted curve when this was shifted by 1.6 eV. The experimental estimate of the Coulomb interaction is then  $U = 1.6 \pm 0.2$  eV [49] as an average over all orbitals and about 1.4 eV for the highest occupied orbital. Since Auger is rather surface sensitive, this number may be more representative for  $U$  at the surface. One can estimate that  $U$  at the surface is about 0.3 eV larger than in the bulk, due to fewer neighbors and less efficient screening [47]. This suggests that the bulk value of  $U$  for the  $t_{1u}$  and  $h_u$  orbitals may be on the order  $U = 1.1$  eV, which is close to the theoretical estimate.  $U$  has also been estimated for  $K_6C_{60}$  in a similar way [50], giving a similar value  $U = 1.5$  eV.

### 5.3 Electron-phonon interaction

The electron-phonon interaction plays an important role for many properties of the alkali-doped fullerides. For instance, superconductivity is believed to be due the electron-phonon interaction. Fig. 5 indicates the different types of phonons in alkali-doped  $C_{60}$  compounds. The low-lying modes are librations (4-5 meV) and intermolecular modes (energies up to about 17 meV) involving alkali- $C_{60}$  and  $C_{60}$ - $C_{60}$  modes. The high-lying modes (34-195 meV) are intramolecular modes, where the molecules are deformed. All the low-lying modes have a rather weak coupling to the  $t_{1u}$  electrons, and the main coupling is to the intramolecular phonons. Here, we

therefore focus on the the coupling to these phonons. These phonons couple primarily to the level energies in contrast to the intermolecular phonons which couple to the hopping integrals. The  $C_{60}$  molecule has  $60 \times 3 - 6 = 174$  intramolecular modes. For symmetry reasons, however, the  $t_{1u}$  electrons only couple to modes with  $A_g$  or  $H_g$  symmetry. There are eight five-fold degenerate  $H_g$  modes and two nondegenerate  $A_g$  modes. The coupling to the  $t_{1u}$ -level takes the form [53]

$$H_{el-ph} = \sum_{\nu=1}^8 g_{\nu} \sum_{M=1}^5 \sum_{\sigma} \sum_{m=1}^3 \sum_{m'=1}^3 \left( V_{H_g}^{(M)} \right)_{mm'} \psi_{m\sigma}^{\dagger} \psi_{m'\sigma} \left( b_{\nu M} + b_{\nu M}^{\dagger} \right) + \sum_{\nu=9}^{10} g_{\nu} \sum_{\sigma} \sum_{m=1}^3 \sum_{m'=1}^3 \left( V_{A_g} \right)_{mm'} \psi_{m\sigma}^{\dagger} \psi_{m'\sigma} \left( b_{\nu} + b_{\nu}^{\dagger} \right), \quad (35)$$

where  $\psi_{m\sigma}^{\dagger}$  creates a  $t_{1u}$  electron with quantum number  $m$  and  $b_{\nu M}^{\dagger}$  creates a phonon in mode  $\nu$  with quantum number  $M$ . The first eight modes are  $H_g$  Jahn-Teller phonons and the next two are  $A_g$  phonons. The coupling constants are  $g_{\nu}$  and the coupling to the  $H_g$  phonons is given by the matrices

$$V_{H_g}^{(1)} = \frac{1}{2} \begin{pmatrix} -1 & 0 & 0 \\ 0 & -1 & 0 \\ 0 & 0 & 2 \end{pmatrix} \quad V_{H_g}^{(2)} = \frac{\sqrt{3}}{2} \begin{pmatrix} 1 & 0 & 0 \\ 0 & -1 & 0 \\ 0 & 0 & 0 \end{pmatrix} \quad V_{H_g}^{(3)} = \frac{\sqrt{3}}{2} \begin{pmatrix} 0 & 1 & 0 \\ 1 & 0 & 0 \\ 0 & 0 & 0 \end{pmatrix} \\ V_{H_g}^{(4)} = \frac{\sqrt{3}}{2} \begin{pmatrix} 0 & 0 & 1 \\ 0 & 0 & 0 \\ 1 & 0 & 0 \end{pmatrix} \quad V_{H_g}^{(5)} = \frac{\sqrt{3}}{2} \begin{pmatrix} 0 & 0 & 0 \\ 0 & 0 & 1 \\ 0 & 1 & 0 \end{pmatrix} \quad (36)$$

and the coupling to the  $A_g$  phonons by

$$V_{A_g}^{(1)} = \begin{pmatrix} 1 & 0 & 0 \\ 0 & 1 & 0 \\ 0 & 0 & 1 \end{pmatrix}. \quad (37)$$

The corresponding dimensionless electron-phonon coupling constant is [53]

$$\lambda = \frac{5}{3} N(0) \sum_{\nu=1}^8 \frac{g_{\nu}^2}{\hbar \omega_{\nu}} + \frac{2}{3} N(0) \sum_{\nu=9}^{10} \frac{g_{\nu}^2}{\hbar \omega_{\nu}}, \quad (38)$$

where  $N(0)$  is the density of states per spin and molecule and  $\omega_{\nu}$  is the frequency of mode  $\nu$ . The theoretical calculation of the electron-phonon coupling for a solid is very complicated. Lannoo *et al.* [54] showed that for intramolecular modes in fullerenes, important simplifications follow from the large difference between the intramolecular ( $E_I$ ) and intermolecular ( $W$ ) energy scales. The coupling for a solid can then be obtained approximately from a calculation for a free molecule and the density of states  $N(0)$  of the solid. Thus, it is sufficient to calculate the shift  $\Delta \varepsilon_{\nu\alpha}$  of the  $t_{1u}$  levels  $\alpha$  for a free  $C_{60}$  molecule per unit displacement of the  $\nu$ th phonon coordinate. One then finds that

$$\lambda \sim N(0) \sum_{\nu\alpha} \frac{\Delta \varepsilon_{\nu\alpha}^2}{\omega_{\nu}^2}. \quad (39)$$

Mode	$\omega_\nu$	$\lambda_\nu/N(0)$						
		Theory			Photoemission		Raman	
		Antrop. [55]	Faul. [56]	Man. [57]	Iwa. [60]	Gun. [58]	Iwa. [60]	Kuz. [61]
$H_g(8)$	1575	.022	.009	.014	.018	.023	.011	.003
$H_g(7)$	1428	.020	.015	.015	.023	.017	.028	.004
$H_g(6)$	1250	.008	.002	.003	.002	.005	.007	.001
$H_g(5)$	1099	.003	.002	.004	.005	.012	.009	.001
$H_g(4)$	774	.003	.010	.004	.006	.018	.007	.003
$H_g(3)$	710	.003	.001	.009	.012	.013	.015	.003
$H_g(2)$	437	.006	.010	.011	.011	.040	.012	.020
$H_g(1)$	273	.003	.001	.005	.006	.019	.007	.048
$\sum H_g$		.068	.049	.065	.083	.147	.096	.083

**Table 9:** Partial electron-phonon coupling constants  $\lambda_\nu/N(0)$  (in eV) according to different theoretical calculations and derived from photoemission and Raman scattering. The energies  $\omega_\nu$  (in  $\text{cm}^{-1}$ ) of the modes for the undoped system are shown.

This gives a molecule-specific quantity which is multiplied by  $N(0)$ . Table 9 shows results for the electron-phonon coupling. The theoretical calculations by Antropov *et al* [55], Faulhaber *et al.* [56] and Manini *et al.* [57] are based on *ab initio* LDA calculations. The work of Iwahara *et al.* is based on the B3LYP functional with some Hartree-Fock exchange mixed in. There are substantial deviations between the distribution of coupling strength to the different modes in the different calculations. This distribution is very sensitive to the precise form of the phonon eigenvectors. The deviations between the total coupling strengths are smaller. The work of Iwahara *et al.* gives a stronger coupling than the other three calculations. This is not so surprising, since this work is based on a rather different functional.

An experimental method for estimating the electron-phonon coupling is the use of photoemission data. Because of the relatively strong electron-phonon coupling, we expect to see satellites due to the excitation of phonons. The weights of the satellites give information about the strength of the coupling. This is essentially the Franck-Condon effect, but because of the Jahn-Teller effect the calculation of the satellite structure is rather complicated. The photoemission spectra of  $\text{K}_3\text{C}_{60}$  and  $\text{Rb}_3\text{C}_{60}$  have been analyzed along these lines [62]. Due to the broadening effects in a solid and due to the complications in the theoretical treatment of bands with dispersion, however, it was not possible to derive reliable, quantitative values for the electron-phonon coupling.

Photoemission spectra have also been measured for free  $\text{C}_{60}^-$  ions. In this case the theoretical treatment is substantially simpler [58]. In these experiments, a beam of  $\text{C}_{60}^-$  ions was created and a photoemission experiment was performed using a laser light source ( $\hbar\omega = 4.025$  eV) and a time of flight spectrometer. The spectrum resulting from emission from the  $t_{1u}$  level was measured. To analyze the results, we use the couplings in Eq. (35) of the  $t_{1u}$  level to the two  $A_g$  and the eight five-fold degenerate  $H_g$  modes. For this model the ground-state can be calculated by numerical diagonalization to any desired accuracy [58]. Furthermore, within

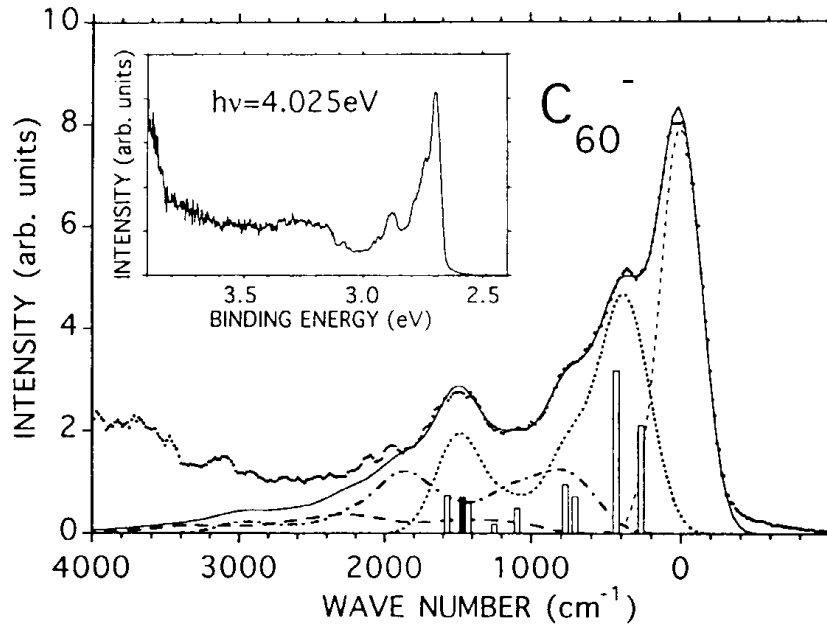


**Fig. 6:** Experimental (dots) and theoretical (full line) photoemission spectrum of  $C_{60}^-$ . The theoretical no-loss (dashed), single-loss (dotted) and double-loss (dashed-dotted) curves are also shown. The contributions of the different modes to the single-loss curve are given by bars ( $H_g$ : open,  $A_g$ : solid). The inset shows the experimental spectrum over a larger energy range (after Gunnarsson *et al.* [58]).

the sudden approximation [63], the photoemission spectrum can easily be calculated. A set of coupling constants is then assumed and the resulting spectrum is compared with experiment. The coupling parameters are varied until good agreement with experiment is obtained, thereby providing an estimate of the couplings. The resulting spectrum is compared with experiment in Fig. 6 and the corresponding parameters are shown in Table 9. An uncertainty in this approach is that with the available resolution, it is not possible to distinguish between the coupling to  $A_g$  modes and  $H_g$  modes with similar energies. The couplings to the  $A_g$  modes were therefore taken from a calculation [55]. With this assumption, the couplings to the  $H_g$  modes can then be determined. An equally good fit can, however, be obtained using other couplings to the  $A_g$  modes if the couplings to the  $H_g$  modes are changed correspondingly.

Substantially later the experiments in Ref. [58] were repeated by Wang *et al.* [59]. It was now possible to obtain a better resolution. These data have been analyzed in a similar way as in Ref. [58] by Iwahara *et al.* [60]. Their results are also shown in Table 9. The total coupling is weaker than in Ref. [58], but still substantially larger than in the *ab initio* LDA calculations. The agreement with the calculation using the B3LYP is better.

Raman scattering provides a different method of estimating the coupling strength. The electron-phonon coupling allows phonons to decay into an electron-hole pair in the metallic fullerenes. This decay contributes to the width of the phonon and can be measured in Raman scattering. Other factors may also contribute to the width, but one can try to eliminate these by subtracting the width of the phonons for a nonmetallic system, where a decay in electron-hole pairs is not

possible. This was done by Winter and Kuzmany [61], and Table 9 shows results adapted [39] from the experiments [61]. The total weight does not differ much from what was obtained from photoemission [60], but the distribution of weight between the different modes differs dramatically. Theoretically, it is found that in the solid there is a transfer of weight to lower modes, due to the coupling to electron-hole pairs [64]. This mechanism is operative for the Raman data but not for the photoemission data (taken for a free molecule). This may explain some of the discrepancy between the photoemission and Raman data.

## 6 Conclusions

For complicated systems with strong correlation effects it is often not possible to obtain accurate *ab initio* solutions, but it is instead useful to turn to models. An important issue is then how to obtain parameters and how to renormalize parameters to include as much physics as possible. We have discussed how the basic principle is to try to include, implicitly as a renormalization of parameters, all effects not explicitly included in the model. On the other hand, we should not allow effects included explicitly in the model to renormalize parameters. For many-body systems there is no general systematic and controlled way of doing this. The basic assumption is often that the electrons can be put into two groups of “fast” (delocalized) and “slow” (localized) electrons, where the “fast” electrons are assumed to adjust to the “slow” electrons, and therefore can be projected out. Such a division is, however, often not very clear cut. Nevertheless some methods have been relatively successful in obtaining parameters for certain classes of systems. We have, however, shown simple examples of many-body effects that are usually not included, but can have an appreciable effect on the parameters. In particular, renormalization effects may work differently for different experiments. We have also argued that it is important to try to extract parameters from different sources, both theory and experiment, to obtain a better understanding of the accuracy of the parameters.

## References

- [1] P. Hohenberg and W. Kohn, Phys. Rev. **136**, B864 (1964)
- [2] W. Kohn and L.J. Sham, Phys. Rev. **140**, A1133 (1965)
- [3] L. Hedin, Phys. Rev. **139**, A796 (1965)
- [4] F. Aryasetiawan and O. Gunnarsson, Reports on Progress in Physics, **61**, 237 (1998)
- [5] P.W. Anderson, Phys. Rev. **124**, 41 (1961)
- [6] J. Hubbard, Proc. Royal Society (London) **276**, 238 (1963)
- [7] F.C. Zhang and T.M. Rice, Phys. Rev. B **37** 3759, (1988)
- [8] A. Iandelli and A. Palenzona: *Crystal chemistry of intermetallic compounds in Handbook on the Physics and Chemistry of Rare Earths*, Vol. 3, Eds.: K.A. Gschneider Jr. and L. Eyring (North-Holland, Amsterdam, 1979) p. 1
- [9] B. Johansson, J. Phys. F **4**, L 169 (1979)
- [10] J.W. Allen and R.M. Martin, Phys. Rev. Lett. **49**, 1106 (1982)
- [11] K. Held, A.K. McMahan and R.T. Scalettar, Phys. Rev. Lett. **87**, 276404 (2001)
- [12] P.O. Löwdin, J. Chem. Phys. **19**, 1396 (1951)
- [13] O.K. Andersen, O. Jepsen and D. Glötzel: *Canonical Description of the Band Structure of Metals.*, in *Highlights of Condensed Matter Theory*, Eds. F. Bassani, F. Fumi and M.P. Tosi (North-Holland, Amsterdam 1985)
- [14] O. Gunnarsson, Phys. Rev. **41**, 514 (1990)
- [15] C. Herring: *Magnetism*, Vol. 4, Eds. G.T. Rado and H. Suhl (Academic Press, New York, 1966)
- [16] B.N. Cox, M.A. Coulter and P. Loyd, J. Phys. F: Metal Physics **4**, 807 (1974)
- [17] J.F. Herbst, R.E. Watson, and J.W. Wilkins, Phys. Rev. B **13**, 1439 (1976) and Phys. Rev. B **17**, 3089 (1978)
- [18] P.H. Dederichs, S. Blügel, R. Zeller, and H. Akai, Phys. Rev. Lett. **53**, 2512 (1984)
- [19] M.S. Hybertsen, M. Schlüter, N.E. Christensen, Phys. Rev. B **39**, 9028 (1989)
- [20] M. Cococcioni and S. de Gironcoli, Phys. Rev. B **71**, 035105 (2005)
- [21] A.K. McMahan, R.M. Martin, S. Satpathy, Phys. Rev. B **38**, 6650 (1988)

- [22] O. Gunnarsson, O.K. Andersen, O. Jepsen, J. Zaanen, Phys. Rev. B **39**, 1708 (1989)
- [23] V.I. Anisimov and O. Gunnarsson, Phys. Rev. B **43**, 7570 (1991)
- [24] Ref. [25] (Sec. IIID) argues that the “cut off” LDA [21, 22] for, e.g., a transition metal, incorrectly includes on-site  $3d$ - $3d$  transitions to describe breathing (cf. Sec. 3.4) of the central  $3d$  orbitals. This is incorrect, since  $3d$ - $3d$  transitions would not change the radial extent of the  $3d$  orbital. It was further implied that metallic  $3d$  screening is included, i.e., transfer of charge to the central  $3d$  orbitals, already included explicitly in the Hubbard model. This is, however, excluded by keeping the total occupancy of the  $3d$  orbitals at the prescribed value. Finally, it was argued that breathing of the  $3d$  orbital should not be included. Since breathing is not explicitly included in the Hubbard model, it should be included in the calculation of  $U$ . It is an important effect [26, 27].
- [25] F. Aryasetiawan, K. Karlsson, O. Jepsen, and U. Schönberger, Phys. Rev. B **74**, 125106 (2006)
- [26] O. Gunnarsson, O.K. Andersen, O. Jepsen, and J. Zaanen, Phys. Rev. B **39**, 1708 (1989)
- [27] O. Gunnarsson and O. Jepsen, Phys. Rev. B **38**, 3568 (1988)
- [28] I.V. Solovyev and M. Imada, Phys. Rev. B **71**, 045103 (2005)
- [29] I.V. Solovyev and P.H. Dederichs, Phys. Rev. B **49**, 6736 (1994)
- [30] J.A. Pople and D.L. Beveridge: *Approximate Molecular Orbital Theory* (McGraw-Hill, New York, 1970), p. 27-29
- [31] M.I. Katsnelson and A.I. Lichtenstein, J.Phys.: Condens. Matter **11**, 1037 (1999) and references therein
- [32] Similar results were found for other system containing atoms from the middle of the  $3d$  series [33].
- [33] V. Drchal, O. Gunnarsson, and O. Jepsen, Phys. Rev. B **44**, 3518 (1991)
- [34] O. Gunnarsson *et al.*, Phys. Rev. B **41**, 4811 (1990)
- [35] J.W. Allen, S.J. Oh, O. Gunnarsson, K. Schönhammer, M.B. Maple, M.S. Torikachvili, and I. Lindau, Adv. Phys. **35**, 275 (1986)
- [36] O.K. Andersen, Phys. Rev. B **12**, 3060 (1975)
- [37] P.W. Anderson, Phys. Rev. Lett. **18**, 1049 (1967)
- [38] O. Gunnarsson and K. Schönhammer, Phys. Rev. B **40**, 4160 (1989)
- [39] O. Gunnarsson, *Alkali-doped Fullerenes* (World Scientific, Singapore, 2004)

- 
- [40] L. Cano-Cortes, A. Dolfen, J. Merino, J. Behler, B. Delley, K. Reuter, and E. Koch, *Eur. Phys. J. B* **56**, 173 (2007)
- [41] W. Harrison, *Electronic structure and the properties of solids*, (Freeman, San Francisco, 1980)
- [42] O. Gunnarsson, S. Satpathy, O. Jepsen, and O.K. Andersen, *Phys. Rev. Lett.* **67**, 3002 (1991)
- [43] O. Gunnarsson, S.C. Erwin, E. Koch, and R.M. Martin, *Phys. Rev. B* **57**, 2159 (1998)
- [44] N. Laouini, O. K. Andersen, and O. Gunnarsson, *Phys. Rev. B* **51**, 17446 (1995)
- [45] V. de Coulon, J.L. Martins, and F. Reuse, *Phys. Rev. B* **45**, 13671 (1992)
- [46] M.R. Pederson and A.A. Quong, *Phys. Rev. B* **46**, 13584 (1992)
- [47] V.P. Antropov, O. Gunnarsson, and O. Jepsen, *Phys. Rev. B* **46**, 13647 (1992)
- [48] R.L. Hettich, R.N. Compton, and R.H. Ritchie, *Phys. Rev. Lett.* **67**, 1242 (1991)
- [49] R.W. Lof, M.A. van Veenendaal, B. Koopmans, H.T. Jonkman, and G.A. Sawatzky, *Phys. Rev. Lett.* **68**, 3924 (1992)
- [50] P.A. Brühwiler, A.J. Maxwell, A. Nilsson, N. Mårtensson, and O. Gunnarsson, *Phys. Rev. B* **48**, 18296 (1993)
- [51] A.F. Hebard, R.C. Haddon, R.M. Fleming, and R. Kortan, *Appl. Phys. Lett.* **59**, 2109 (1991)
- [52] A.F. Hebard, *Phys. Today* **45**, No. 11, p. 26 (1992)
- [53] O. Gunnarsson, *Phys. Rev. B* **51**, 3493 (1995)
- [54] M. Lannoo, G.A. Baraff, M. Schlüter, and D. Tomanek, *Phys. Rev. B* **44**, 12106 (1991)
- [55] V.P. Antropov, O. Gunnarsson, and A.I. Liechtenstein, *Phys. Rev. B* **48**, 7651 (1993)
- [56] J.C.R. Faulhaber, D.Y.K. Ko, and P.R. Briddon, *Phys. Rev. B* **48**, 661 (1993)
- [57] N. Manini, A.D. Corso, M. Fabrizio, and E. Tosatti, *Phil. Mag. B* **81**, 793 (2001)
- [58] O. Gunnarsson, H. Handschuh, P.S. Bechthold, B. Kessler, G. Ganteför, and W. Eberhardt, *Phys. Rev. Lett.* **74**, 1875 (1995)
- [59] X.B. Wang, H.K. Woo, and L.S. Wang, *J. Chem. Phys.* **123**, 051106 (2005)
- [60] N. Iwahara, T. Sato, K. Tanaka, L.F. Chibotaru, *Phys. Rev. B* **82**, 245409 (2010)
- [61] J. Winter and H. Kuzmany, *Phys. Rev. B* **53**, 655 (1996)

- [62] M. Knupfer, M. Merkel, M.S. Golden, J. Fink, O. Gunnarsson, V.P. Antropov, Phys. Rev. B **47**, 13944 (1993)
- [63] L. Hedin and S. Lundqvist, in *Solid State Physics*, Vol. 23, p. 1, Eds. H. Ehrenreich, D. Turnbull, and F. Seitz (Academic, New York, 1969)
- [64] J.E. Han and O. Gunnarsson, Phys. Rev. B **61**, 8628 (2000)